~~D0 Note #3028~~
DOConf-96-12

# The Dijet Mass Spectrum and Angular Distributions with the DØ Detector

The DØ Collaboration[1]
(June 25, 1996)

We present preliminary results from an analysis of dijet data collected during the 1994-95 Tevatron Collider run with an integrated luminosity of 91 $pb^{-1}$. Measurements of dijet mass spectra and dijet angular distributions in $\bar{p}p$ collisions at $\sqrt{s}$ = 1.8 TeV are compared with next-to-leading order QCD theory.

S. Abachi,[14] B. Abbott,[28] M. Abolins,[25] B.S. Acharya,[43] I. Adam,[12] D.L. Adams,[37] M. Adams,[17] S. Ahn,[14] H. Aihara,[22] J. Alitti,[40] G. Álvarez,[18] G.A. Alves,[10] E. Amidi,[29] N. Amos,[24] E.W. Anderson,[19] S.H. Aronson,[4] R. Astur,[42] R.E. Avery,[31] M.M. Baarmand,[42] A. Baden,[23] V. Balamurali,[32] J. Balderston,[16] B. Baldin,[14] S. Banerjee,[43] J. Bantly,[5] J.F. Bartlett,[14] K. Bazizi,[39] J. Bendich,[22] S.B. Beri,[34] I. Bertram,[37] V.A. Bezzubov,[35] P.C. Bhat,[14] V. Bhatnagar,[34] M. Bhattacharjee,[13] A. Bischoff,[9] N. Biswas,[32] G. Blazey,[14] S. Blessing,[15] P. Bloom,[7] A. Boehnlein,[14] N.I. Bojko,[35] F. Borcherding,[14] J. Borders,[39] C. Boswell,[9] A. Brandt,[14] R. Brock,[25] A. Bross,[14] D. Buchholz,[31] V.S. Burtovoi,[35] J.M. Butler,[3] W. Carvalho,[10] D. Casey,[39] H. Castilla-Valdez,[11] D. Chakraborty,[42] S.-M. Chang,[29] S.V. Chekulaev,[35] L.-P. Chen,[22] W. Chen,[42] S. Choi,[41] S. Chopra,[24] B.C. Choudhary,[9] J.H. Christenson,[14] M. Chung,[17] D. Claes,[42] A.R. Clark,[22] W.G. Cobau,[23] J. Cochran,[9] W.E. Cooper,[14] C. Cretsinger,[39] D. Cullen-Vidal,[5] M.A.C. Cummings,[16] D. Cutts,[5] O.I. Dahl,[22] K. De,[44] M. Demarteau,[14] N. Denisenko,[14] D. Denisov,[14] S.P. Denisov,[35] H.T. Diehl,[14] M. Diesburg,[14] G. Di Loreto,[25] R. Dixon,[14] P. Draper,[44] J. Drinkard,[8] Y. Ducros,[40] S.R. Dugad,[43] D. Edmunds,[25] J. Ellison,[9] V.D. Elvira,[42] R. Engelmann,[42] S. Eno,[23] G. Eppley,[37] P. Ermolov,[26] O.V. Eroshin,[35] V.N. Evdokimov,[35] S. Fahey,[25] T. Fahland,[5] M. Fatyga,[4] M.K. Fatyga,[39] J. Featherly,[4] S. Feher,[14] D. Fein,[2] T. Ferbel,[39] G. Finocchiaro,[42] H.E. Fisk,[14] Y. Fisyak,[7] E. Flattum,[25] G.E. Forden,[2] M. Fortner,[30] K.C. Frame,[25] P. Franzini,[12] S. Fuess,[14] E. Gallas,[44] A.N. Galyaev,[35] T.L. Geld,[25] R.J. Genik II,[25] K. Genser,[14] C.E. Gerber,[14] B. Gibbard,[4] V. Glebov,[39] S. Glenn,[7] J.F. Glicenstein,[40] B. Gobbi,[31] M. Goforth,[15] A. Goldschmidt,[22] B. Gómez,[1] G. Gomez,[23] P.I. Goncharov,[35] J.L. González Solís,[11] H. Gordon,[4] L.T. Goss,[45] N. Graf,[4] P.D. Grannis,[42] D.R. Green,[14] J. Green,[30] H. Greenlee,[14] G. Griffin,[8] N. Grossman,[14] P. Grudberg,[22] S. Grünendahl,[39] W.X. Gu,[14,*] G. Guglielmo,[33] J.A. Guida,[2] J.M. Guida,[5] W. Guryn,[4] S.N. Gurzhiev,[35] P. Gutierrez,[33] Y.E. Gutnikov,[35] N.J. Hadley,[23] H. Haggerty,[14] S. Hagopian,[15] V. Hagopian,[15] K.S. Hahn,[39] R.E. Hall,[8] S. Hansen,[14] R. Hatcher,[25] J.M. Hauptman,[19] D. Hedin,[30] A.P. Heinson,[9] U. Heintz,[14] R. Hernández-Montoya,[11] T. Heuring,[15] R. Hirosky,[15] J.D. Hobbs,[14] B. Hoeneisen,[1,†] J.S. Hoftun,[5] F. Hsieh,[24] Tao Hu,[14,*] Ting Hu,[42] Tong Hu,[18] T. Huehn,[9] S. Igarashi,[14] A.S. Ito,[14] E. James,[2] J. Jaques,[32] S.A. Jerger,[25] J.Z.-Y. Jiang,[42] T. Joffe-Minor,[31] H. Johari,[29] K. Johns,[2] M. Johnson,[14] H. Johnstad,[29] A. Jonckheere,[14] M. Jones,[16] H. Jöstlein,[14] S.Y. Jun,[31] C.K. Jung,[42] S. Kahn,[4] G. Kalbfleisch,[33] J.S. Kang,[20] R. Kehoe,[32] M.L. Kelly,[32] L. Kerth,[22] C.L. Kim,[20] S.K. Kim,[41] A. Klatchko,[15] B. Klima,[14] B.I. Klochkov,[35] C. Klopfenstein,[7] V.I. Klyukhin,[35] V.I. Kochetkov,[35] J.M. Kohli,[34] D. Koltick,[36] A.V. Kostritskiy,[35] J. Kotcher,[4]

[1]Submitted to the 28th International Conference on High Energy Physics, Warsaw, Poland, 25-31 July 1996.

J. Kourlas,[28] A.V. Kozelov,[35] E.A. Kozlovski,[35] M.R. Krishnaswamy,[43] S. Krzywdzinski,[14] S. Kunori,[23] S. Lami,[42] G. Landsberg,[14] J-F. Lebrat,[40] A. Leflat,[26] H. Li,[42] J. Li,[44] Y.K. Li,[31] Q.Z. Li-Demarteau,[14] J.G.R. Lima,[38] D. Lincoln,[24] S.L. Linn,[15] J. Linnemann,[25] R. Lipton,[14] Y.C. Liu,[31] F. Lobkowicz,[39] S.C. Loken,[22] S. Lökös,[42] L. Lueking,[14] A.L. Lyon,[23] A.K.A. Maciel,[10] R.J. Madaras,[22] R. Madden,[15] L. Magaña-Mendoza,[11] S. Mani,[7] H.S. Mao,[14,*] R. Markeloff,[30] L. Markosky,[2] T. Marshall,[18] M.I. Martin,[14] B. May,[31] A.A. Mayorov,[35] R. McCarthy,[42] T. McKibben,[17] J. McKinley,[25] T. McMahon,[33] H.L. Melanson,[14] J.R.T. de Mello Neto,[38] K.W. Merritt,[14] H. Miettinen,[37] A. Mincer,[28] J.M. de Miranda,[10] C.S. Mishra,[14] N. Mokhov,[14] N.K. Mondal,[43] H.E. Montgomery,[14] P. Mooney,[1] H. da Motta,[10] M. Mudan,[28] C. Murphy,[17] F. Nang,[5] M. Narain,[14] V.S. Narasimham,[43] A. Narayanan,[2] H.A. Neal,[24] J.P. Negret,[1] E. Neis,[24] P. Nemethy,[28] D. Nešić,[5] M. Nicola,[10] D. Norman,[45] L. Oesch,[24] V. Oguri,[38] E. Oltman,[22] N. Oshima,[14] D. Owen,[25] P. Padley,[37] M. Pang,[19] A. Para,[14] C.H. Park,[14] Y.M. Park,[21] R. Partridge,[5] N. Parua,[43] M. Paterno,[39] J. Perkins,[44] A. Peryshkin,[14] M. Peters,[16] H. Piekarz,[15] Y. Pischalnikov,[36] V.M. Podstavkov,[35] B.G. Pope,[25] H.B. Prosper,[15] S. Protopopescu,[4] D. Pušeljić,[22] J. Qian,[24] P.Z. Quintas,[14] R. Raja,[14] S. Rajagopalan,[42] O. Ramirez,[17] M.V.S. Rao,[43] P.A. Rapidis,[14] L. Rasmussen,[42] S. Reucroft,[29] M. Rijssenbeek,[42] T. Rockwell,[25] N.A. Roe,[22] P. Rubinov,[31] R. Ruchti,[32] J. Rutherfoord,[2] A. Sánchez-Hernández,[11] A. Santoro,[10] L. Sawyer,[44] R.D. Schamberger,[42] H. Schellman,[31] J. Sculli,[28] E. Shabalina,[26] C. Shaffer,[15] H.C. Shankar,[43] R.K. Shivpuri,[13] M. Shupe,[2] J.B. Singh,[34] V. Sirotenko,[30] W. Smart,[14] A. Smith,[2] R.P. Smith,[14] R. Snihur,[31] G.R. Snow,[27] J. Snow,[33] S. Snyder,[4] J. Solomon,[17] P.M. Sood,[34] M. Sosebee,[44] M. Souza,[10] A.L. Spadafora,[22] R.W. Stephens,[44] M.L. Stevenson,[22] D. Stewart,[24] D.A. Stoianova,[35] D. Stoker,[8] K. Streets,[28] M. Strovink,[22] A. Sznajder,[10] P. Tamburello,[23] J. Tarazi,[8] M. Tartaglia,[14] T.L. Taylor,[31] J. Thompson,[23] T.G. Trippe,[22] P.M. Tuts,[12] N. Varelas,[25] E.W. Varnes,[22] P.R.G. Virador,[22] D. Vititoe,[2] A.A. Volkov,[35] A.P. Vorobiev,[35] H.D. Wahl,[15] G. Wang,[15] J. Warchol,[32] G. Watts,[5] M. Wayne,[32] H. Weerts,[25] A. White,[44] J.T. White,[45] J.A. Wightman,[19] J. Wilcox,[29] S. Willis,[30] S.J. Wimpenny,[9] J.V.D. Wirjawan,[45] J. Womersley,[14] E. Won,[39] D.R. Wood,[29] H. Xu,[5] R. Yamada,[14] P. Yamin,[4] C. Yanagisawa,[42] J. Yang,[28] T. Yasuda,[29] P. Yepes,[37] C. Yoshikawa,[16] S. Youssef,[15] J. Yu,[14] Y. Yu,[41] Q. Zhu,[28] Z.H. Zhu,[39] D. Zieminska,[18] A. Zieminski,[18] E.G. Zverev,[26] and A. Zylberstejn[40]

[1]Universidad de los Andes, Bogotá, Colombia
[2]University of Arizona, Tucson, Arizona 85721
[3]Boston University, Boston, Massachusetts 02215
[4]Brookhaven National Laboratory, Upton, New York 11973
[5]Brown University, Providence, Rhode Island 02912
[6]Universidad de Buenos Aires, Buenos Aires, Argentina
[7]University of California, Davis, California 95616
[8]University of California, Irvine, California 92717
[9]University of California, Riverside, California 92521
[10]LAFEX, Centro Brasileiro de Pesquisas Físicas, Rio de Janeiro, Brazil
[11]CINVESTAV, Mexico City, Mexico
[12]Columbia University, New York, New York 10027
[13]Delhi University, Delhi, India 110007
[14]Fermi National Accelerator Laboratory, Batavia, Illinois 60510
[15]Florida State University, Tallahassee, Florida 32306
[16]University of Hawaii, Honolulu, Hawaii 96822
[17]University of Illinois at Chicago, Chicago, Illinois 60607
[18]Indiana University, Bloomington, Indiana 47405
[19]Iowa State University, Ames, Iowa 50011
[20]Korea University, Seoul, Korea

[21]Kyungsung University, Pusan, Korea
[22]Lawrence Berkeley National Laboratory and University of California, Berkeley, California 94720
[23]University of Maryland, College Park, Maryland 20742
[24]University of Michigan, Ann Arbor, Michigan 48109
[25]Michigan State University, East Lansing, Michigan 48824
[26]Moscow State University, Moscow, Russia
[27]University of Nebraska, Lincoln, Nebraska 68588
[28]New York University, New York, New York 10003
[29]Northeastern University, Boston, Massachusetts 02115
[30]Northern Illinois University, DeKalb, Illinois 60115
[31]Northwestern University, Evanston, Illinois 60208
[32]University of Notre Dame, Notre Dame, Indiana 46556
[33]University of Oklahoma, Norman, Oklahoma 73019
[34]University of Panjab, Chandigarh 16-00-14, India
[35]Institute for High Energy Physics, 142-284 Protvino, Russia
[36]Purdue University, West Lafayette, Indiana 47907
[37]Rice University, Houston, Texas 77251
[38]Universidade Estadual do Rio de Janeiro, Brazil
[39]University of Rochester, Rochester, New York 14627
[40]CEA, DAPNIA/Service de Physique des Particules, CE-SACLAY, France
[41]Seoul National University, Seoul, Korea
[42]State University of New York, Stony Brook, New York 11794
[43]Tata Institute of Fundamental Research, Colaba, Bombay 400005, India
[44]University of Texas, Arlington, Texas 76019
[45]Texas A&M University, College Station, Texas 77843

## I. INTRODUCTION

The production of hadronic jets is the dominant contribution to high transverse momentum ($p_T$) processes in proton–antiproton ($\bar{p}p$) collisions. High $p_T$ jets were observed since the early phase of experimentation at the CERN $\bar{p}p$ collider and their production properties are well described by perturbative QCD (1). Predictions for the inclusive jet cross section (and hence the inclusive dijet cross section) have been made using next–to–leading order (NLO) QCD (2–4). These $\mathcal{O}({\alpha_s}^3)$ calculations, which include the possibility of a third radiated parton, reduce theoretical uncertainties to 10–20%. We measure the inclusive dijet mass spectrum and the dijet angular distribution in the DØ detector (5) at the Fermilab Tevatron Collider at $\sqrt{s} = 1.8$ TeV. Both measurements, when compared to NLO, constitute a rigorous test of QCD. Previous measurements of the dijet mass distribution (6) and the dijet angular distribution (7) have been presented by the CDF collaboration.

## II. JET AND EVENT SELECTION

Jet detection in the DØ detector primarily requires the uranium–liquid argon calorimeters which cover pseudorapidity $|\eta| \leq 4$ ( $\eta = -\ln(\tan(\theta/2))$ where $\theta$ is the polar angle of the object relative to the proton beam). The calorimeters have electromagnetic and hadronic single particle resolutions of $15\%/\sqrt{E}$ and $50\%/\sqrt{E}$, respectively. They are transversely segmented into projective towers of $\Delta\eta \times \Delta\phi = 0.1 \times 0.1$ and have longitudinal segmentation of eight to eleven segments depending on $\eta$. The electromagnetic modules (EM) include the first four longitudinal segments and the coarse hadronic modules (CH) the final longitudinal

segment. The intervening segments comprise the fine hadronic modules and the intercryostat detectors. The total calorimetric depth exceeds seven nuclear interaction lengths for $|\eta| \leq 0.5$. The calorimeters are also segmented into trigger tiles of $\Delta\eta \times \Delta\phi = 0.8 \times 1.6$ and trigger towers of $\Delta\eta \times \Delta\phi = 0.2 \times 0.2$, where $\phi$ is azimuthal angle. The event vertex is determined using tracks reconstructed in the central tracking system. The detector includes two trigger scintillator hodoscopes located on each side of the interaction region at $1.9 < |\eta| < 4.3$. Timing distributions of particles traversing the two hodoscopes indicate the occurrence of a single inelastic interaction or of multiple inelastic interactions during a single beam–beam crossing.

Event selection occurred in two hardware stages and a final software stage. The initial hardware trigger selected an inelastic particle collision as indicated by the hodoscopes. The next trigger stage required transverse energy above a preset threshold in the calorimeter trigger tiles. Selected events are then digitized and sent to an array of processors. Jet candidates are then reconstructed with a fast cone algorithm and the entire event logged to tape if any jet $E_T$ exceeded a specified threshold. During the 1994–1995 data run, the software jet thresholds were 30, 50, 85, and 115 GeV with integrated luminosities of 0.355, 4.56, 51.7 and 90.7 $pb^{-1}$ respectively. To avoid saturating the data acquisition bandwidth, only a fraction of the lower threshold triggers were accepted.

Jets are reconstructed offline using an iterative jet cone algorithm with a cone radius of $\mathcal{R}$=0.7 in $\eta$–$\phi$ space (8). The algorithm uses preclusters formed from 1 GeV seed towers. The jet $E_T$ is defined as the sum of each cell $E_T$ within the cone. The $E_T$ –weighted rapidity and azimuth of the jet are calculated and the center of the cone repositioned on this axis. The jet $E_T$ and direction are then recalculated until the cone direction is stable. The final jet directions are calculated using the components of the jet energy vector. After all jets are formed, closely spaced jets which share more than 50% of the smaller jet energy are merged; otherwise, the energy is split evenly between the two, and the directions accordingly recalculated. For the 1994–1995 data, prior to reconstruction, isolated energetic cells (mainly due to calorimeter noise) were removed from the event. Removal occurred for 3% of 100 GeV jets and for 10% of 350 GeV jets. In some cases this procedure removed energy that was not due to noise. To correct for this any removed cell located within $\mathcal{R}$=0.7 of a jet axis was restored to the jet if the cell had no more than 50% of the final, restored jet energy. The restored jet rapidity was recalculated with the $E_T$ weighted rapidity of the jet and restored cell.

Background jets from isolated noisy calorimeter cells and accelerator losses are eliminated with quality cuts. The fraction of energy detected in the EM modules for any jet must lie between 5 and 95%. Also the ratio of energy in the second most energetic cell in a jet to the most energetic cell must be greater than 0.10 (this cut is not imposed on jets which include restored cells). Background from the Main Ring accelerator passing through the CH modules is eliminated by requiring that the fraction of the jet energy in the CH modules be less than 40%. It is required that the two leading $E_T$ jets pass these quality cuts for the event to be accepted. Background from cosmic ray bremsstrahlung is eliminated by requiring the magnitude of the summed transverse energy in an event, $|\not\!\!E_T|$, to be less than 70% of the leading jet $E_T$. Residual contamination from the backgrounds is estimated to be less than 2% at all $E_T < 500$ GeV based on Monte-Carlo simulations and scanning of all very high jet $E_T$ candidates (9). The overall jet selection efficiency for $|\eta| \leq 0.5$ has been

measured as a function of jet $E_T$ and found to be 97±1% below 250 GeV and 94±1% at 400 GeV.

At high instantaneous luminosity more than one interaction in a single beam crossing is probable. The event reconstruction retains, at most, two vertices. The quantity $\mathcal{H}_T = |\Sigma_{\mathbf{jets}} \vec{E}_T^{\,\mathbf{jet}}|$ was calculated for both vertices. The vertex with the minimum $\mathcal{H}_T$ is selected as the event vertex and used to calculate jet $E_T$ and $\eta$. The selected vertex is also required to be within 50 cm of the detector center. The $z$ requirement is 90 ± 1% efficient, independent of $E_T$.

## III. ENERGY CALIBRATION

The transverse energy of each jet has been corrected for offsets, $O$, due to underlying events and noise/zero suppression; the fraction of particle energy showering, $S$, outside the jet cone; and calorimeter hadronic energy response, $R$. The corrected jet energy, $E_{\mathbf{jet}}$, can be related to the measured energy, $E_{\mathbf{meas}}$, by $E_{\mathbf{jet}} = [E_{\mathbf{meas}} - O]/[(1 - S) * R]$. The offsets, $O$, to jet energy are extracted from the energy densities as a function of $\eta$ for single and double minimum bias events. The single interaction energy deposition is due to a single underlying event and to noise/zero suppression ($U+N$). The double interaction deposition is due to *two* underlying events and the noise/zero suppression ($2U+N$). The $\eta$ dependent functions $U$ and $N$ are then used to subtract the energy offsets on a jet–by–jet basis. The underlying interaction correction for each jet is determined by the average number of interactions expected for the instantaneous luminosity observed at the time the jet was recorded.

The out–of–cone showering correction, $S$, should compensate for energy (from particles emitted within the cone) that leaks outside the cone during calorimeter showering. This puts the experimental measure of jet energy on identical footing as the theoretical NLO treatment which includes parton radiation inside the cone. Similarly, $S$ must compensate for particles emitted outside the cone but which deposit some energy inside. The energy spectrum for jets was simulated with HERWIG and the pattern of energy deposition at the cell level for each particle taken from a sample of single particle showers collected at a test beam (5). After reconstruction with the 0.7 cone algorithm and for jets in the central unit of rapidity, negligible energy flow was measured across the jet cone boundary.

The hadronic response correction, $R$, is based on the $\not\!\!E_T$ balance in a photon–jets event sample, after the jets are corrected for offset. The photon candidates, designated "$\gamma$", include direct photons and jets with a high $\pi^0/\eta$ fraction that have fragmented into photons. The response of the calorimeter to electrons is linear to $\leq$ 1% for energies above 10 GeV (10). The absolute electromagnetic calibration is determined using dielectron and diphoton decays of the $Z$ (11), $J/\psi$, and $\pi^0$ resonances. The "$\gamma$" candidates are selected by requiring a reconstructed electromagnetic deposition above 8 GeV, candidate isolation, and shower shape consistent with that of a test beam electron (10). The latter two requirements ensure that these "$\gamma$" candidates have electromagnetic response, whether they are photons or photon–like jets. The hadronic response for "$\gamma$"–jet events can be derived from data using the conservation of momentum: $R = 1 + [\hat{n_{T\gamma}} \cdot \hat{\not\!\!E}_T]/E_{T\gamma}$, where $\hat{n_{T\gamma}}$ and $E_{T\gamma}$ are the transverse direction vector and energy of the $\gamma$ and $\hat{\not\!\!E}_T$ is the missing $E_T$ vector. Figure

1 shows the measured hadronic response, $R$, as a function of $E' = E_{T\gamma} \cdot \cosh(\eta_{\rm jet})$, the expected jet energy if all the hadronic energy were contained in a single jet at the leading jet rapidity $\eta_{\rm jet}$. The most energetic jets are located in the forward calorimeter. A 3% response correction between the central and forward calorimetry was included, determined by direct comparison of the response of equal energy jets in the two regions. Figure 1 also shows the measured leading jet energy, $E_{\rm meas}$, as a function of $E'$. Together, the two curves provide the relationship between $E_{\rm meas}$ and $R$.

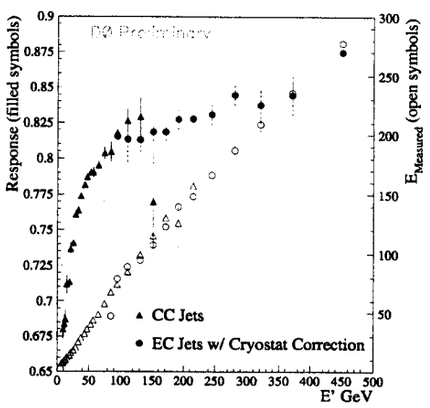


**FIG. 1.** Jet response (left axis, filled symbols) and measured jet energy (right axis, open symbols) versus $E'$. Data from the central (triangles) and end calorimeters (circles) are included.

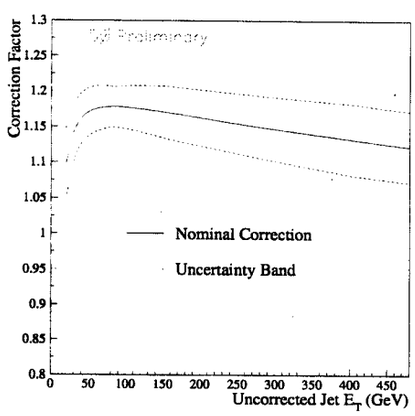


**FIG. 2.** The jet energy scale correction factor as a function of uncorrected jet energy. The upper and lower curves represent the total uncertainty.

The response, $R$, is directly measured with data for $E_{\rm meas}$ less than 350 GeV and is extended to higher energies using full GEANT simulated $\gamma$–jet events. Figure 2 shows the mean total jet correction as a function of $E_T$ for $|\eta| \leq 0.5$. The upper and lower curves represent the correction uncertainty. Errors due to additional soft radiation in the event and statistical errors from the high $E_T$ simulation have been included.

## IV. INCLUSIVE DIJET MASS DISTRIBUTION

For each event that passes the quality cuts the dijet mass can be calculated, assuming that the jets are massless, using the relationship; $M_{jj}{}^2 = 2 \cdot E_T{}^1 \cdot E_T{}^2 \cdot (\cosh(\Delta\eta) - \cos(\Delta\phi))$. Each event is weighted by the efficiency of the quality cuts applied to the data.

The inclusive dijet mass cross sections are computed for two partially overlapping pseudorapidity ranges: $|\eta|_{1,2} < 1.0$, $\Delta\eta < 1.6$ ($|\eta|_{1,2} < 0.5$), in contiguous mass ranges: 200, 270, 370, 500 (200, 220, 330, 420) GeV, corresponding to the various software jet thresholds. The relative normalizations of the four trigger sets are established by requiring equal cross–sections in the regions where two trigger sets overlap and are efficient. The adjustments are 0.0±0.0, 2.8±1.3%, 5.7±1.5%, and 6.3±1.6% for the four mass regions used in this analysis.

The final observed cross section corrected for jet and event selection efficiency is shown in Fig. 3. The combined systematic errors are also shown in Fig 3. ranging from ~13% at 200 GeV to ~55% at 950 GeV. The systematic error is dominated by the uncertainty due to the energy scale with smaller contributions due to jet selection (1%), vertex selection (1%), the vertex cut (1%), the luminosity scale (8%) and the luminosity matching.

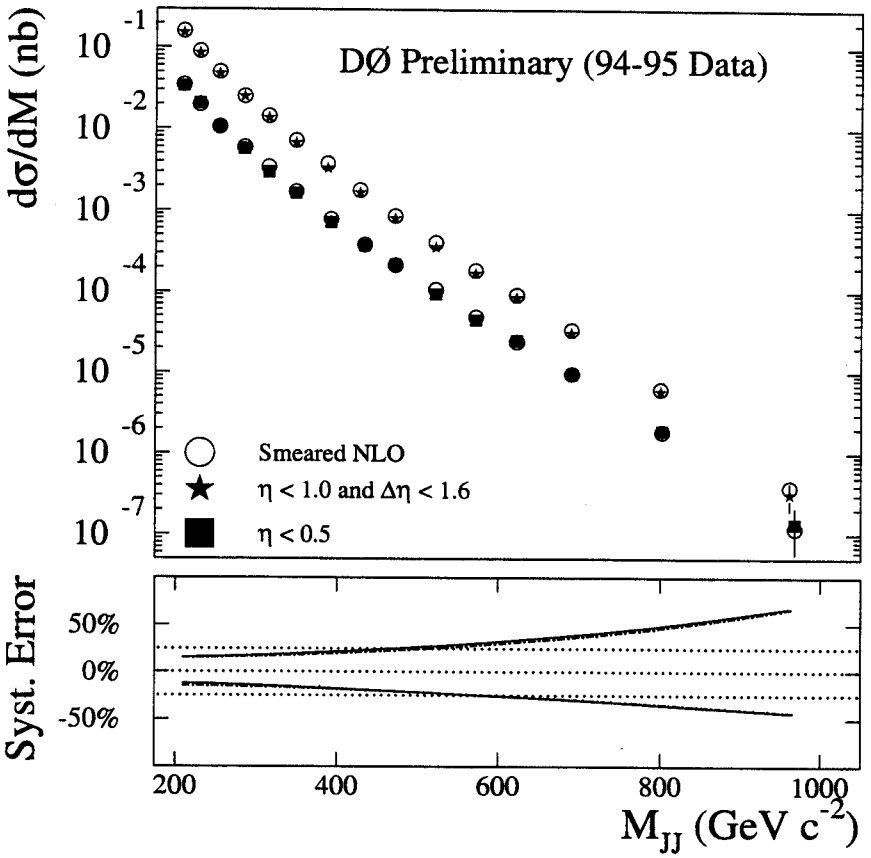


**FIG. 3.** $d^2\sigma/dM_{jj}d\eta$ for $|\eta|_{1,2} < 1.0$, $\Delta\eta < 1.6$ ($|\eta|_{1,2} < 0.5$). The inset solid (dash-dot) curves represent the plus and minus $1\sigma$ systematic errors (the dotted lines show the 0, ±25% levels).

Figure 3 also shows a prediction for the inclusive dijet mass spectrum from the NLO parton event generator JETRAD (2). The NLO calculation of the dijet mass spectrum has been smeared by the measured jet resolutions. There is good agreement between the prediction and the data over seven orders of magnitude. The data and theoretical calculation are binned identically in $M_{jj}$ bins. The NLO calculation requires specification of the renormalization and factorization scale ($\mu = E_T/2$ where $E_T$ is the maximum jet $E_T$ in the generated event), parton distribution function (CTEQ2ML (12)), and a parton clustering algorithm. Partons within 1.3 $\mathcal{R}$ of one another were clustered if they were also within $\mathcal{R}$=0.7 of their $E_T$ weighted $\eta, \phi$ centroid. The value of 1.3 $\mathcal{R}$ was determined by over-

laying jets in data from separate events and determining the separation at which the jet reconstruction algorithm could resolve the individual jets. Variation of the pdf can alter the prediction by up to 20% depending on $M_{jj}$. Variation of $\mu$ between $0.25E_T$ to $E_T$ can alter the predictions normalization by 10–20% with some $M_{jj}$ dependence. In addition the choice of parton clustering between 1.3 $\mathcal{R}$ and 2.0 $\mathcal{R}$ alters the normalization by $\sim$ 5% with a small (2–3%) $M_{jj}$ dependence.

Figure 4 shows the ratio, $(D-T)/T$, for the data ($D$) and the NLO theoretical predictions based on the CTEQ2ML (12) and MRSD0′ (13) pdf's. Given the experimental and theoretical uncertainties the predictions are in excellent agreement with the data. The CTEQ2ML pdf gives the best agreement for the absolute normalization.

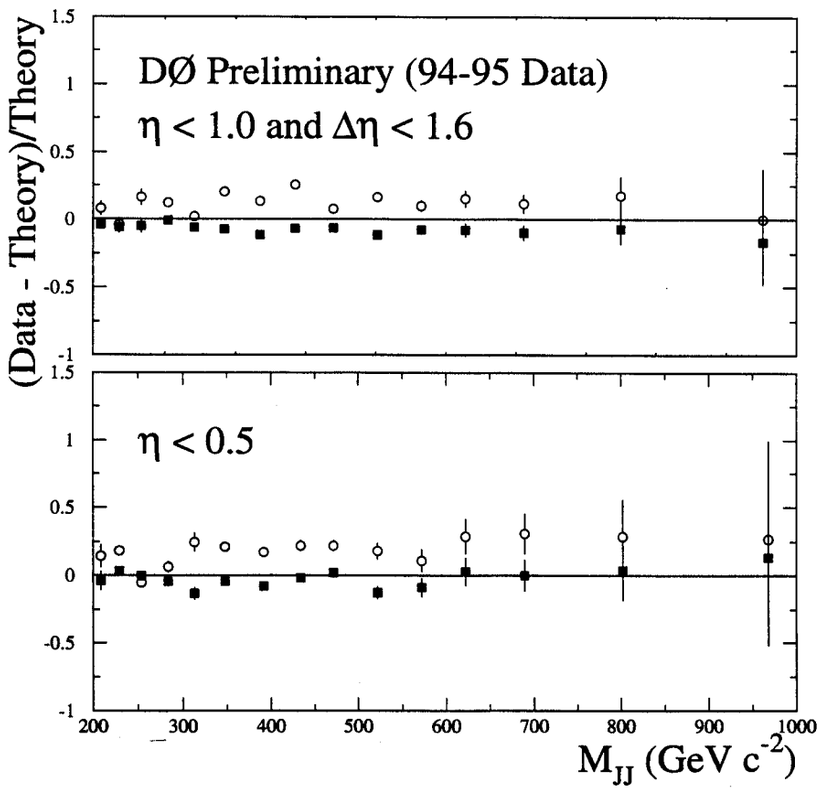


**FIG. 4.** The difference between the data and the smeared NLO QCD predictions normalized to the theoretical prediction ($(D-T)/T$). The solid (open) symbols represent the calculation using the CTEQ2ML (MRSD0′) pdf's.

## V. DIJET ANGULAR DISTRIBUTION

Measured in the dijet center of mass, the dijet angular distribution is sensitive primarily to the QCD matrix elements, and relatively insensitive to the parton distribution functions. Therefore, we can measure the properties of parton-parton scattering without strong dependence on the details of the parton distribution functions. Moreover, the angular dependence of the $qg \to qg$, $q\bar{q} \to q\bar{q}$, and $gg \to gg$ processes are similar.

At small center of mass scattering angles, the dijet angular distribution predicted by leading order QCD is proportional to the Rutherford cross section: $d\hat{\sigma}_{ij}/d\cos\theta^* \sim 1/\sin^4(\frac{\theta^*}{2})$. It is useful to measure the angular distribution in the variable $\chi$, rather than $cos\theta^*$, where $\chi = (1+\cos\theta^*/1-\cos\theta^*) = e^{|\eta_1-\eta_2|}$. The dijet angular distribution is plotted in the variable $\chi$ in order to flatten out the distribution and facilitate an easier comparison to theory (14).

The quantity measured in the dijet angular analysis is $1/N(dN/d\chi)$, which is measured in bins of the dijet mass $M_{jj}$. The other variables of interest are the center-of-mass pseudorapidity, $\eta^* = \frac{1}{2}(\eta_1 - \eta_2)$, and the pseudorapidity boost: $\eta_{\mathbf{boost}} = \frac{1}{2}(\eta_1 + \eta_2)$. The two leading $E_T$ jets were required to have a maximum pseudorapidity ($\eta_{\mathbf{max}}$) less than 3.0. Four mass bins were then chosen so that the trigger used to collect the data is 100% efficient whilst maximizing the statistics and $\chi$ reach ($\chi_{\mathbf{max}}$). Once the value of $\chi_{\mathbf{max}}$ is chosen then a cut is made on the $\eta_{\mathbf{boost}}$ of the dijet system so that there is uniform acceptance for the $\chi$ range being examined. The boost cut is kept at 1.5 for all mass bins for simplicity, although a larger boost cut is possible for some mass bins. The mass, $\chi$, and $\eta_{\mathbf{boost}}$ ranges are described in table 1.

| Min $E_{T1}$ | Mass | | | $\chi_{\mathbf{max}}$ | $\lvert\eta^*_{\mathbf{max}}\rvert$ | $\lvert\eta_{\mathbf{boost\_max}}\rvert$ |
|---|---|---|---|---|---|---|
| 55 | 260 | – | 425 | 20 | 1.5 | 1.5 |
| 120 | 475 | – | 635 | 13 | 1.3 | 1.5 |
| 120 | 550 | + | | 18 | 1.45 | 1.5 |
| 175 | 635 | + | | 11 | 1.2 | 1.5 |

**TABLE 1.** The mass bins and their $\chi$ and $\eta$ ranges.

The dijet angular distribution is relatively insensitive to many systematic effects. Unlike the dijet mass spectrum, the dijet angular distribution shows little effect due to the overall energy scale. However, since $\chi$ depends on $\Delta\eta$ directly, it is very sensitive to $\eta$ dependent quantities. The effects of multiple interactions and an $\eta$ dependent energy scale are the two dominant sources of error in this analysis. The approximate size of each systematic error is shown in table 2.

The leading order and next to leading order theory was calculated using JETRAD (2). The dijet angular distributions were calculated using an inclusive cross section with $|\eta| < 3.5$ and $40.0 < E_T < 500.0$ GeV. The extended $\eta$ range and the lowered $E_T$ cut were used in order to allow for 3 $\sigma$ of smearing in $E_T$ as well as $\eta$. The CTEQ3M parton distribution functions were used with a renormalization scale of $E_T/2$ of the leading $E_T$ jet. The theory was smeared in $E_T$ and $\eta$ in order to compare it to data, although as shown in the previous

| Systematic Study | Approximate % Effect |
|---|---|
| Statistical Error | $\sim 5\%$ |
| Multiple Interactions | $\sim 8\%$ |
| Jet Quality | $\sim 1\%$ |
| Jet Quality Efficiencies | $\sim 1\%$ |
| Missing $E_T$ | $\sim 1\%$ |
| Vertex | $\sim 1\%$ |
| Split/Merge Events | $\sim 2\%$ |
| Energy Scale Correction | $\sim 2\%$ |
| $E_T$ and $\eta$ Smearing | $\sim 2\%$ |
| $\eta$-bias | $\sim 2\%$ |
| $\eta$ dependent energy scale | $\sim 10\%$ |

**TABLE 2.** Sources and sizes of the systematic errors in the dijet angular distributions.

table, the effect of $E_T$ and $\eta$ smearing is small. Four mass ranges are shown compared to the LO and NLO predictions of QCD in Fig 5. The "wiggles" in the theoretical predictions are due to statistical fluctuations in the JETRAD calculation. We see that the NLO predictions agree better with the the data $\chi$ distributions than the LO predictions. Finally, Fig 6 demonstrates the effects of varying the renormalization/factorization scale at NLO on the dijet angular distributions. For the scale values studied only a small variation to the NLO predictions is observed.

## VI. CONCLUSION

In conclusion, we have measured the inclusive dijet mass spectrum for $|\eta|_{1,2} < 1.0$, $\Delta\eta < 1.6$ ($|\eta|_{1,2} < 0.5$) and $200 < M_{jj} < 1100$ GeV at $\sqrt{s} = 1.8$ TeV. The QCD NLO model, using two different pdf's is in excellent agreement with the $M_{jj}$ dependent shape of the observed inclusive dijet mass spectrum. We have also measured the dijet angular distribution which also agrees well with QCD NLO predictions in all mass bins.

## ACKNOWLEDGMENTS

We thank W. Giele, E. Glover, and D. Kosower for their helpful comments and suggestions. We thank the staffs at Fermilab and the collaborating institutions for their contributions to the success of this work, and acknowledge support from the Department of Energy and National Science Foundation (U.S.A.), Commissariat à L'Energie Atomique (France), Ministries for Atomic Energy and Science and Technology Policy (Russia), CNPq (Brazil), Departments of Atomic Energy and Science and Education (India), Colciencias (Colombia), CONACyT (Mexico), Ministry of Education and KOSEF (Korea), CONICET and UBACyT (Argentina), and the A.P. Sloan Foundation.

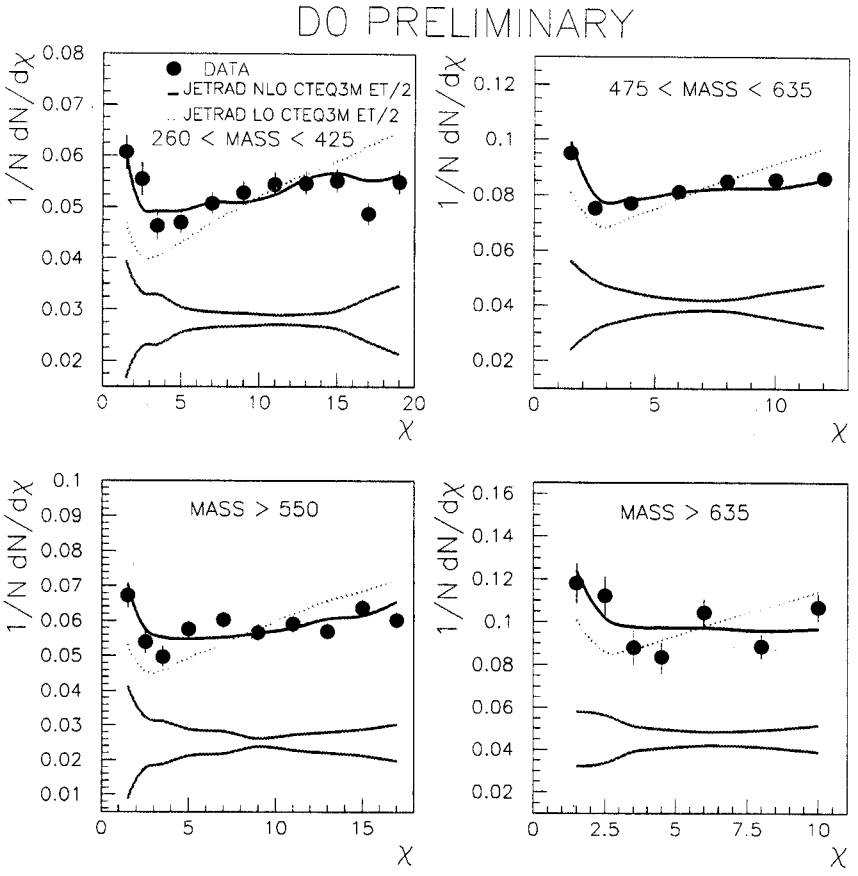


**FIG. 5.** Comparisons of data to NLO and LO predictions of QCD using JETRAD with CTEQ3M and a renormalization scale of $E_T/2$. The errors bars are statistical. Shown at the bottom of each plot is the plus and minus $1\sigma$ systematic error band.

## REFERENCES

* Visitor from IHEP, Beijing, China.
† Visitor from Univ. San Francisco de Quito, Ecuador.

1. P. Bagnia and S. D. Ellis, **Ann. Rev. Nucl. Part. Sc. 38** (1988) 659.
2. W.T. Giele, E.W. Glover, and D.A.Kosower, Phys. Rev. Lett. **73**, 2019 (1994)and private communications. We use the program JETRAD written by these authors.
3. S.D. Ellis, Z. Kunszt, and D.E. Soper, Phys. Rev. Lett. **64**, 2121 (1990.)
4. F. Aversa, et al., Phys. Rev. Lett. **65**, (1990)
5. S. Abachi et al., (DØ Collaboration), Nucl. Instr. Meth. **A338**, 185 (1994)
6. F. Abe et al., (CDF Collaboration), Phys. Rev. **D41**, 1722 (1990)
7. F. Abe et al., (CDF Collaboration), Phys. Rev. Lett. **69**, 2896 (1992)
   A. Bhatti, *Inclusive Jet Production at Tevatron*, FERMILAB-CONF-95-192-E, Jun 1995. 12pp. Presented at 10th Topical Workshop on Proton-Antiproton Collider Physics, Batavia, IL, 9-13 May 1995.

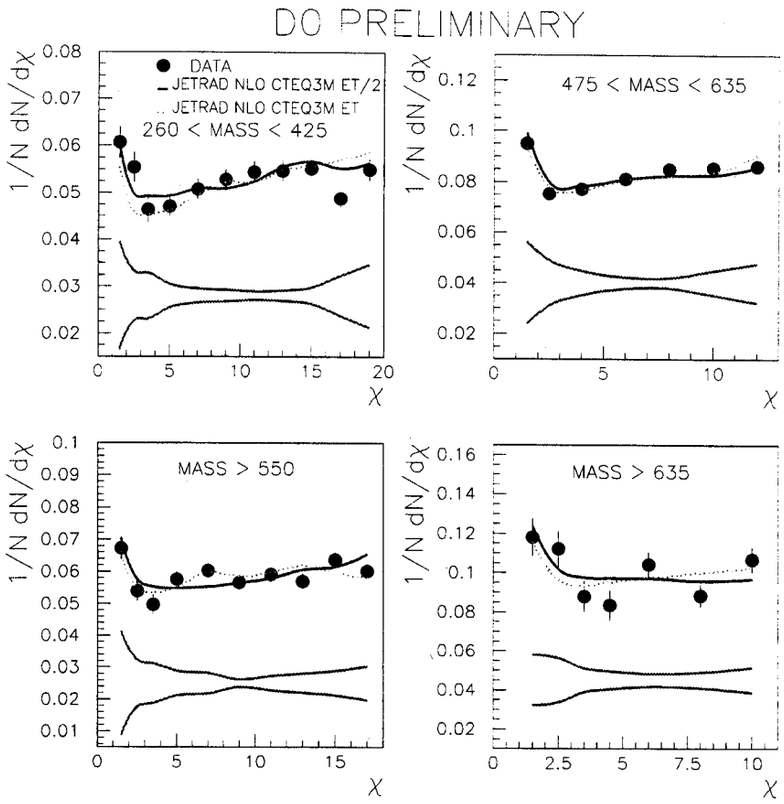


**FIG. 6.** Comparisons of data to NLO predictions of QCD using JETRAD with CTEQ3M and renormalization scales of $E_T/2$ and $E_T$. The error bars are statistical. Shown at the bottom of each plot is the plus and minus $1\sigma$ systematic error band.


8. S. Abachi et al., (DØ Collaboration), Phys. Lett. **B257**, 232 (1995)
9. D. Elvira, *Measurement of the Inclusive Jet Cross Sections at* $\sqrt{s} = 1.8 TeV$ *with the DØ Detector*, Ph.D. Thesis, (1993)
10. J. Kotcher (for the DØ Collaboration), Proceedings of the 1994 Beijing Calorimetry Symposium, IHEP - Chinese Acadamy of Sciences, Beijing, China (October, 1994) p144.
11. P. Renton, "Precision Tests of Electroweak Theories", Lepton–Photon Conference, Beijing, Beijing, P.R. China (1995), OUNP–95–20.
12. J. Botts et al., (CTEQ Collaboration), Phys. Rev. **D51**, 4763 (1994)
    J. Botts et al., (CTEQ Collaboration), Phys. Lett. **B304**, 159 (1993)
13. A.D. Martin, R.G. Roberts, and W.J. Stirling, Phys. Lett. **B306**, 145 (1993) and erratum Phys. Lett. **B309**, 492 (1993)
14. R. K. Ellis and W. J. Stirling, 'QCD and Collider Physics', FERMILAB-Conf-90/164-T, August 1990, p. 66-69.